Observation of Vortex Packets in Direct Numerical Simulation of Fully Turbulent Channel Flow

R. J. Adrian and Z. C. Liu

Laboratory for Turbulence and Complex Flow, Department of Theoretical and Applied Mechanics
University of Illinois at Urbana-Champaign, Urbana, Illinois 61801, USA

Abstract: A number of experimental studies have inferred the existence of packets of inclined, hairpin-like vortices in wall turbulence on the basis of observations made in two-dimensional x-y planes using visualization and particle image velocimetry (PIV). However, there are very few observations of hairpins in existing three-dimensional studies made using direct numerical simulation (DNS), and no such study claims to have revealed packets. We demonstrate, for the first time, the existence of hairpin vortex packets in DNS of turbulent flow. The vortex packet structure found in the present study at low Reynolds number, $Re_\tau = 300$, is consistent with and substantiates the observations and the results from two-dimensional PIV measurements at higher Reynolds numbers in channel, pipe and boundary layer flows. Thus, the evidence supports the view that vortex packets are a universal feature of wall turbulence, independent of effects due to boundary layer trips or critical conditions in the aforementioned numerical studies. Visualization of the DNS velocity field and vortices also shows the close association of hairpin packets with long low-momentum streaks and the regions of high Reynolds shear stress.

Keywords: Wall turbulence, Wall eddies, Structure, Hairpin vortices, Hairpin vortex packets, Direct numerical simulation

1. Introduction

Despite the passage of nearly one-half century since Theodorsen's (1952) proposal that hairpin vortices constitute one of the primary flow mechanisms of wall turbulence, the existence and importance of hairpin (or horseshoe) vortices remains an unsettled subject. Opinions in the community that studies wall turbulence range from comfortable acceptance of the hairpin paradigm to non-acceptance. Among those who do allow for hairpins in the mechanical picture of wall turbulence there is sometimes serious doubt about their importance, either as stress-associated events or as mechanisms that lead to the formation of events that are important to the creation of turbulent stresses. Clearly, this situation derives from a lack of convincing evidence, especially at high Reynolds number. The difficulty lies partly in the full three-dimensionality of the hairpin structure, partly in the problem of defining a vortex, and partly in the multi-scale complexity of these flows.

In his exhaustive study of the structure of wall turbulence, Robinson (1991) identified arches of vorticity and long regions of quasi-stream-wise vorticity, but stopped short of embracing the view that these elements were connected in the form of hairpins. On the basis of flow visualization of boundary layers using smoke and a laser light sheet in a low speed wind

tunnel, Head and Bandyopadhyay (1981) concluded that the boundary layer flow is full of hairpin vortices. They rose from the wall with an inclination approximately 45° to the wall and a width of about one hundred viscous wall units. Smith and co-workers (1984, 1991) have also visualized patterns that appeared to be hairpins with H_2 bubbles and dyes, but doubts always lingered because the vorticity could not be measured in the visualizations. Recently, Chacin, Cantwell, and Kline (1996) have reported observing three-dimensional hairpin shapes in turbulent channel flow simulated by DNS, providing some of the best evidence to date for the existence of such structures, albeit at low Reynolds number.

Contemporaneously, experimental and numerical studies by the present authors and co-workers have lead to a structural model in which an important element of the turbulent wall layer is not just the hairpin vortex, but vortices that are grouped together in stream-wise-aligned packets that grow upwards at a characteristic angle with respect to the wall in the range of $\gamma = 5–15°$, cf. Fig.1. A packet exists if the vortices within in it propagate with small velocity dispersion, so that their spatial arrangement has a long lifetime. The vortices in these packets may be classified as hairpins, provided that a sufficiently liberal interpretation is given to the term. Thus, while the packet in Fig. 1 is perfectly symmetric, most vortices that occur in fully turbulent flows are asymmetric with legs of unequal strength, and they are often distorted by the motions of other vortices. Their coherent alignment creates an induced backflow region inside the packet that is much longer than the backflow induced by a single vortex, thus explaining the extraordinarily long correlation length of the stream-wise momentum, as observed by Grant (1958) and Townsend (1976). The grouping of the vortices also explains the occurrence of multiple second-quadrant events in turbulent bursts, as documented by Bogard and Tiederman (1986), Luchik and Tiederman, 1987) and Tardu (1995), and the lift-up/oscillation/violent ejection sequence of events observed in a turbulent burst (c.f. Robinson, 1991 for a review).

The hairpin vortex packet paradigm finds precedence in the earlier pioneering studies by Head and Bandyopadhyay (1981) and Smith (1984). Both observed two or more hairpins occurring in stream-wise alignment in natural turbulent boundary layers. Smith's (1984) H2-bubble visualizations were at low Reynolds number close to the wall, while Head and Bandyopadhyay's (1981) observations of inclined packets were principally at the interface between a smoke-filled, moderate Reynolds number boundary layer and the clean free stream.

By examining the signatures of the hairpins vortices, the recent two-dimensional PIV experiments of Adrian, Meinhart and Tomkins (2000) (hereafter referred to as AMT 2000) reveal that moderate Reynolds number turbulent wall flow is densely populated with hairpin-shaped vortices grouped into coherent vortex packets. Two-dimensional PIV experiments find multiple zones of nearly uniform stream-wise momentum, suggesting that the boundary layer is made up of a hierarchy of vortex packets. The younger packets are located near the wall, while the older packets are larger and occupy space farther away from the wall. Wide-angle, two-dimensional PIV measurements at moderate Reynolds number document the geometry of full vortex packets. Their shapes vary, but the characteristic angle of growth is common, and the experiments provide evidence that the vortex packets are a frequently occurring coherent structure.

Smith et al. (1991) offer a model that explains the mechanisms of self-induction that can lead a single hairpin to form a packet of hairpins, and Zhou et al. (1996, 1998, 1999) independently found the process of auto-generation of new vortices by numerical simulation of a single vortex at low Reynolds number ($Re_\tau = 150$) in an otherwise clean turbulent channel flow. An initial hairpin-like structure generated by stochastic estimation based on two-point correlation of velocities was put into a mean turbulent velocity profile and allowed to evolve. When the strength of the initial structure was above a threshold, it developed and formed a primary hairpin, and subsequently generated secondary and tertiary hairpins and later a downstream hairpin, as shown in Fig. 1. These hairpin vortices organize themselves into a coherent packet aligned in the

stream-wise direction. The complete Navier-Stokes mechanisms for the generation of vortex packets agreed with the most of the model of Smith et al. (1991), although Zhou et al. (1996, 1998, 1999) also predicted a threshold intensity of the primary vortex that is required to initiate auto-generation.

Although the PIV experiments (at moderate Reynolds number and in several different flow apparatus) indicate frequent occurrence of vortex packets in fully turbulent flows, and the numerical/theoretical studies of the evolution of a single hairpin suggest mechanisms by which vortex packets can be formed, there are still some missing threads in the fabric of the evidence. First, the simulations of Zhou et al. (1996, 1998, 1999) were at a Reynolds number that was close to transition, raising questions about the extension of these concepts to higher Reynolds number. Second, hairpin packets have not been reported in direct numerical simulations of fully turbulent flow. This is not, perhaps, surprising, since even the visualization of single hairpins in the complex environment of a fully turbulent flow is a careful study that has only been accomplished recently (Chacin, Cantwell and Kline, 1996). Even so, it is important to clarify this question. If hairpin vortex packets cannot be found in fully turbulent DNS, it could mean that the inference of hairpins from the two-dimensional PIV data is incorrect, or that imperfections in real flow fields (wall roughness, vibrations, inlet disturbances, etc.) favor the production of packets, while the perfect conditions of direct numerical simulations discriminate against their formation. On the other hand, if hairpin packets can be found in fully turbulent direct numerical simulations, the case for their universal nature, independent of secondary factors, is strengthened considerably.

The present DNS of fully developed turbulent channel flows has been performed at Re_τ = 300, twice the Reynolds number of the Zhou et al. (1996, 1998, 1999) simulations. We find that packets with mostly asymmetric hairpin vortices can be observed in both halves of the channel flow for every realization of the present DNS. They occur frequently in both space and time. The observations are consistent with previous two-dimensional PIV experiments in boundary layer and channel flows and with the DNS study of the growth of a packet out of an individual hairpin. The three-dimensional capability of DNS data provides three-dimensional information for the packet structure and characteristics and a clearer picture than the two-dimensional visualizations. The present DNS study also observes a close association of packets with Q2 and Q4 events, long low-momentum streaks and the generation to Reynolds stress.

2. Direct Numerical Simulation

The simulation of fully developed channel flow was performed by solving the full three-dimensional time-dependent Navier-Stokes equations using the pseudo-spectral code originally developed by Lyons et al (1991). The Reynolds number, Re_τ, based on the half channel height, h, and the friction velocity, $u_\tau = \sqrt{(\nu \partial U/\partial y|wall)}$, was 300, where ν was the kinematic viscosity. Periodic boundary conditions were imposed in the stream-wise and span-wise directions, and no-slip and no-penetration conditions held at both walls. The pseudo-spectral method used Fourier series expansions in the stream-wise (x) and span-wise (z) directions and Chebychev polynomial series expansions in the wall-normal (y) direction, and spatial derivatives of the velocity field were computed in spectral space. The algorithm made use of a time-splitting technique in three fractional steps to compute the non-linear convective term, the pressure term and the viscous term of the Navier-Stokes equations. The details of the algorithm have been described in Lyons et al. (1991).

The computational domain in the stream-wise, span-wise and wall-normal directions was 3800^+ x 1900^+ x 600^+ in wall units (ν/u_τ) with grid numbers of 256 x 256 x 129, giving approximately 8.5 million data points. The grid spacing in wall units was 14.9 and 7.49 in x^+ and z^+, and it ranged from 0.09 ~ 7.36 in y^+.

3. Evolution of Vortex Packets at Re_τ=300

The evolution of a single hairpin into a packet of vortices has been computed for the present Reynolds number using procedures identical to those described in Zhou et al. (1996, 1998, 1999). Here, and throughout this paper, we visualize vortices using level surfaces of the swirling strength, as defined in Zhou et al. (1996, 1998, 1999). This flow pattern analysis is based on the critical point concepts of Perry and Chong (1987), Chong et al. (1990). The eigenvalues of the velocity gradient tensor of incompressible flow for every grid point in the flow field are obtained by solving the characteristic equation, $\lambda^3 + Q\lambda + R = 0$, where Q and R are the tensor invariants that determine the local flow pattern. The discriminant is $D = (27/4)\, R^2 + Q^3$. For $D \leq 0$ eigenvalues are real. For $D > 0$ there are one real and two complex conjugate eigenvalues. In this case the flow pattern exhibits stable focus/stretching ($R < 0$) or unstable focus/compressing ($R > 0$). Zhou et al. (1996, 1998, 1999) defined the swirling strength to be the imaginary part of the complex conjugate eigenvalue, λ_{ci}, a new kinematic quantity representing swirling rate around the axis of principal stretching/compression. Surfaces of non-zero constant swirling strength are much like surfaces of constant enstrophy, except that they exclude pure shear, which implies zero swirling strength. The use of swirling strength has the main advantage of avoiding regions of shearing motions that have small swirl, but strong vorticity.

The computations at $Re_\tau = 300$ began with an eddy, shown in Fig. 2, that was found by stochastically estimating the conditional average of the flow field surrounding a second-quadrant (Q2) event at y^+=49. Due to sampling error in forming the two-point spatial correlations needed for the stochastic estimate, the initial eddy contained an asymmetry of approximately 5 per cent with respect to reflections about the x-y mid-plane. The initial condition used by Zhou et al. (1996, 1998, 1999) was perfectly symmetric, so it led to the symmetric pattern in Fig. 1. For comparison, the initial condition for the $Re_\tau = 300$ computation was also symmetrized about the x-y plane, and it was found that a pattern similar to Fig. 1 resulted. Doubling the Reynolds number produced no significant change in the pattern of the eddies in the hairpin packet.

As shown previously (Zhou et al., 1999), asymmetric events grow more rapidly than symmetric events, so they are likely to be the most common form found in natural wall turbulence. To explore this effect the residual asymmetry in Fig. 2 was allowed to remain, with the result that the surprisingly complicated packet shown in Fig 3 evolved out of the relatively minor asymmetry. This packet contains many hairpins that have the form of a cane or a one-legged hairpin. It gives clear meaning to the liberal sense in which hairpins are defined by Zhou et al. (1999). The growth angle of the packet is about γ=15°, similar to the results for the symmetric packets. It contains about five clear hairpins, plus several that are only partially formed. As the evolution of the packet progresses, a considerable amount of interaction occurs by self-induction, leading to many small-scale vortices that create a complicated and apparently chaotic picture that makes identification of the main hairpins difficult. Nevertheless, they can be seen clearly without need of special eduction methods. In fact, eduction is an inferior method of visualizing these structures, because it smoothes the data too much. For this reason, we use visualization of individual structures throughout this paper as the preferred method of demonstrating properties of the packets.

It must be emphasized that the principal difference between the packets in Fig. 2 and Fig, 3 is due to the initial asymmetry, and not the higher Reynolds number.

4. Hairpin Vortex Packets in Fully Turbulent Flow

We next consider the results of simulating the fully turbulent flow in the channel. A portion of a typical turbulent realization is visualized on a sub-domain having dimensions 950^+ x 475^+, and half of the channel height, 300^+ using iso-surfaces of enstrophy, $|\omega|$, in Fig. 4(a) and

swirling strength, λ_{ci}, in Fig. 4(b). The volume of the sub-domain in Fig. 4 is 1/32 of the volume of the whole computational domain. Comparison of Fig. 4(a) and Fig. 4(b) shows that swirling strength captures vortices that contain concentrated vorticity, but discards the shearing motions, making visualization much easier. In the view looking downstream from above, vortices are seen to concentrate in groups that are aligned in the stream-wise direction. Two groups reside in the middle half of the span, and there are indications of a portion of a group at the left and right edges. The character of the vortices in these groups is difficult to determine from this view.

Figure 5(a) is a side-view that shows quasi-streamwise vortices extending along the wall and gradually tilting up at an angle of 30 ~ 45 degrees. This pattern recurs frequently, and it is easy to conclude that it is strong characteristic of the flow. The inclined vortices may be hairpin legs. In Fig. 5(b) hairpin heads (or 'arches', in the terminology of Robinson, 1991) can be seen, and some of them are clearly attached to inclined vortices, forming a cane or a hairpin. The heads of some of the inclined vortices may not visible because their swirling strength falls below the value used to render the images. Thus, one sees many inclined vortices that appear to terminate in the flow. Decreasing the swirling strength level used for the visualization makes the heads of these inclined vortices visible, but it also increases the background clutter, making it difficult to see the other structures. Hence, the value of swirling strength used in the volume renderings is a compromise.

Despite the clarity achieved by visualizing the vortices using the swirling strength (compare Fig. 4(a) to 4(b)), the three-dimensional visualizations in Fig. 4(b) and Fig. 5 are disappointingly difficult to interpret. To make the most reliable identification of a hairpin, we have found it best to first visualize the two-dimensional flow in the *x-y* plane, as in Fig. 6. This also makes it possible to relate the DNS flow fields to the results of other studies such as the planar PIV study in AMT (2000) and the planar visualization of DNS data in Guenther et al. (1998). Signatures of hairpins can be observed in the typical flow field shown in Fig. 6. Hairpin heads appear as span-wise vortices in the *x-y* plane roughly located on a line inclined about 11 degrees with the wall. Below the vortex heads a strong low-momentum flow occurs as a result of collective pumping effect by the hairpin legs and heads in the packet. The low-momentum fluid from each hairpin meets the high momentum fluid from the outer region of the channel and forms stagnation points and a shear layer.

The structure in Fig. 6 is a hairpin packet comprised of at least four hairpin vortices. A three-dimensional schematic of the hairpin vortex packet paradigm is shown in Fig. 7(a). The reader can see how an *x-y* section though the middle of a three-dimensional packet like that depicted in Fig. 7(a) would result in a pattern like that in Fig. 6. The younger hairpins in a packet are the smaller ones that are located upstream with smaller inclination to the wall; the larger hairpins that are located downstream with larger tilt angles are the older ones. Packet structures occur frequently throughout the DNS database in a region between the wall and about $0.6h$. They are typically about $3–6h$ long in the stream-wise direction. They occur less frequently above $0.6h$, but they can sometimes reach beyond the center of the channel. The alignment of the vortices allows the back-induced flow from each hairpin to feed into the succeeding hairpin, creating long, low-momentum streaks. These streaks have also been observed in the *x-z* plane with similar length in stream-wise direction (Liu et al., 1998). The spanwise spacing of neighboring streaks close to the wall, ranging from 100 to 200 wall units, clearly associates them with the classical low speed streaks first observed by Kline et al. (1967). The spanwise spacing grows linearly with distance from the wall.

Having unambiguously located the heads of the hairpins in a view such as Fig 6, it is possible to return to the three-dimensional visualization and highlight those vortices, as shown in Fig. 7(b). The pattern of a packet of growing hairpin vortices now becomes clear. There are still many vortices cluttering the background, but a succession of increasingly taller and wider

hairpins is quite evident. The view in Fig. 7(c) makes the spanwise growth more evident. Applying this method to many different samples from the DNS database consistently yields similar results. In this way, the coherent hairpin vortex pattern can be extracted from the complex pattern of vortices in the background. One can ask where these other vortices arise. One answer lies in Fig. 3 which shows that the internal dynamics of an auto-generating hairpin packet are capable of creating complexity that is similar to that observed in the fully turbulent channel flow. In addition, the large packets move faster than the smaller packets, so that there is a continual series of vortex cut-and-connect interactions as the younger hairpins are overrun by the older ones.

The three-dimensional pattern in Fig. 7(c) provides a fundamental insight into the nature of hairpin packet growth. The mean width of the young packet is about 100–200 wall units, and the hairpin heads grow wider at an angle of 10~12° in the spanwise direction. This angle is nearly the same as the rate of growth in the wall-normal direction, suggesting that the growth of the hairpins is approximately self-similar as they age. The logarithmic variation of the mean velocity is probably associated with the length scale (width or height) increasing with y, causing the back-induced velocity, and hence the mean velocity gradient, to decrease as y^{-1}.

By examining packets at subsequent times we have found that whole packets convect downstream as a coherent structure with little dispersion, so that they exist as slowly evolving patterns for many hundred viscous time scales. The convection velocity of the packet in Fig. 7 is about $12u_\tau$, or 76% of the bulk velocity of the channel.

Tomkins (1997) and Tomkins and Adrian (1999) showed that as a packet grows larger a new, smaller packet very often occurs below it. A similar phenomenon occurs in the DNS, cf. Fig 6. In this manner, a hierarchy of packets forms with older packets residing above younger ones.

Figure 8 shows the eddy structure across the entire channel. Hairpin packets can be seen growing from each wall, and interacting near the centerline. This illustrates a fundamental difference between boundary layer turbulence and channel flow turbulence. In the former, one only has packets growing up from the wall, with no interference from other vortices at the outer edge. In channel flow, the packets experience perturbations from their natural, auto-induced growth mechanism due to vortices from the other side of the channel. These interactions increase the complexity of the pattern, making channel flow somewhat more difficult to visualize and understand.

Inboard of a hairpin the quasi-stream-wise legs and the hairpin head pump low-momentum fluid away from the wall, creating the ejection events. On the outboard sides of the legs and above the head high momentum fluid is pumped downward from the outer region of the channel, and sweeps, i.e. Q4 events, occur. These Q2 and Q4 events contribute strongly to the mean Reynolds stress. Indeed, they appear to be the main source of turbulent friction in wall turbulence. The collective actions of the Q2 and Q4 events from successive hairpins in the packets create long streaks of large Reynolds shear stress. Thus, the shear stress contours, labeled red in Fig. 9, form long streaky regions that lie inside and outside of the packet. This may explain recent observations by Hommema (2001) that show that a large fraction of the turbulent shear stress comes from very low wave numbers in the streamwise co-spectrum of u–v.

5. Conclusions

After sufficient time has elapsed, small asymmetry in the initial pattern used to seed the growth of an auto-generating hairpin packet leads to a complex pattern bordering on chaos. Earlier work with asymmetric initial conditions in AMT (2000) showed that the preferred form of hairpin vortex is the cane shape, rather than a symmetric hairpin. But, by extending the time of the computation, one finds that both canes and symmetric hairpins occur in a very complicated

pattern. This pattern bears many similarities to the patterns observed in fully turbulent simulations, suggesting that much of the randomness in channel flow turbulence is actually inherent in the dynamics of hairpin vortex packets.

The present study presents results that provide clear evidence for the existence of hairpin packets in fully turbulent DNS channel flow. Although a few previous DNS studies showed the existence of individual hairpin vortices (cf. Chacin et al. 1996), the present study, for the first time, reveals the existence and the frequent occurrence of hairpin packets in DNS of wall turbulence. The present observations of the structure and the characteristics of the coherent packets are consistent with and substantiate the previous observations from two-dimensional PIV experiments by AMT (2000) and Tomkins, and Adrian et al. (1998) for boundary layer flows, and the evolution study in DNS channel flow by Zhou et al. (1999).

Acknowledgments

This work was supported by grants from the United States National Science Foundation, NSF ATM 95-22662 and the Office of Naval Research, N00014-99-1-0188. The support and computational facilities of University of Illinois National Center for Supercomputer Applications, Urbana-Champaign are gratefully acknowledged.

References

Adrian, R. J., Balachandar, S. and Tomkins, C. D., The Structure of Vortex Packets in Wall Turbulence. AIAA 98-2962 (1998).

Adrian, R. J., Meinhart, C. D. and Tomkins, C. D., Vortex Organization in the Outer Region of Turbulent Boundary Layers, Journal of Fluid Mechanics, 422 (2000), 1-53.

Bogard, D. G. and Tiederman, W. G., Burst Detection with Single-Point Velocity Measurements, Journal of Fluid Mechanics, 162 (1986), 389-413.

Chacin, J. M., Cantwell, B. J. and Kline, S. J., Study of Turbulent Boundary Layer Structure Using the Invariants of the Velocity Gradient Tensor, Experimental Thermal and Fluid Science, 13 (1996), 308-317.

Chong, M. S., Perry, A. E. and Cantwell, B. J., A General Classification of Three-Dimensional Flow Fields, Physics of Fluids, A2 (1990), 765-777.

Guenther, A., Papavassiliou, D. V., Warholic, M. D. and Hanratty, T. J., Turbulent Flow in a Channel at a Low Reynolds Numbers, Experiments in Fluids, 25 (1998), 503-511.

Grant, H. L., The Large Eddies of Turbulent Motion, Journal of Fluid Mechanics, 4 (1958), 149.

Head, M. R. and Bandyopadhyay, P. B., New Aspects of Turbulent Boundary-Layer Structure, Journal of Fluid Mechanics, 107 (1981), 297-338.

Hommema, S. E., Very Large Scale Motion in Wall-Bounded Turbulence, Ph.D. thesis, University of Illinois, Urbana, Illinois, USA (2001).

Kline, S. J., Reynolds, W. C., Schroub, F. A. and Rundstadler, P. W., The Structure of Turbulent Boundary Layers, Journal of Fluid Mechanics, 12 (1967), 741.

Liu, Z. C., Adrian, R. J. and Hanratty, T. J., A Study of Streaky Structure in a Turbulent Channel Flow with Particle Image Velocimetry, 8th International Symposium on Applications of Laser Techniques to Fluid Mechanics, Lisbon, (1996), 17.1.1-17.1.9.

Luchik, T.S. and Tiederman, W.G., Time-Scale and Structure of Ejections and Bursts in Turbulent Channel Flows, Journal of Fluid Mechanics, 174 (1987), 529-552.

Lyons, S. L., Hanratty, T. J. and McLaughlin, J. B., Large-Scale Computer Simulation of Fully Developed Turbulent Channel Flow with Heat Transfer, International Journal of Numerical Methods in Fluids, 13 (1991), 999-1028.

Meinhart, C. D. and Adrian, R. J., On the Existence of Uniform Momentum Zones in a Turbulent Boundary Layer, Physics of Fluids, 7 (1995), 694-696.

Perry, A. E and Chong, M. S., A Description of Eddying Motions and Flow Patterns Using Critical-Point Concepts, Annual Reviews Fluid of Mechanics, (1987), 125-155.

Robinson, S. K., Coherent Motion in the Turbulent Boundary Layer, Annual Reviews Fluid of Mechanics, 23 (1991), 601-639.

Smith, C. R., A Synthesized Model of the Near-Wall Behavior in Turbulent Boundary Layers. In Proceedings of the 8th Symposium on Turbulence (ed. J. Zakin and G. Patterson) (1984), 299-325, Univ. Missouri-Rolla, Rolla, Missouri.

Smith, C. R., Walker, J. D. A., Haidari, A. H. and Sobrun, U., On the Dynamics of Near-Wall Turbulence, Philosophical Transactions of the Royal Society of London A, 336 (1991), 131-175.

Tardu, S., Characteristics of Single and Clusters of Bursting Events in the Inner Layer, Part 1: Vita Events. Experiments in Fluids, 20 (1995), 112-124.

Theodorsen, T., Mechanism of Turbulence. In Proc. 2nd Midwestern Conference on Fluid Mech., (1952), 1-19, Ohio State University, Columbus, Ohio.

Tomkins, C. D. and Adrian, R. J., Characteristics of Vortex Packets in Wall Turbulence, In Turbulence and Shear Flow Phenomena , eds. S. Bannerjee and J. Eaton (1999), 31-36, Begell House, New York.

Tomkins, C. D., A Particle Image Velocimetry Study of Coherent Structures in a Turbulent Boundary Layer, M.S. thesis, (1997) University of Illinois, Urbana, Illinois, USA.

Townsend, A. A., The Structure of Turbulent Shear Flow. 2nd edition, (1976) Cambridge University Press, Cambridge.

Zhou, J., Meinhart, C. D., Balachandar, S. and Adrian, R. J., Formation of Coherent Hairpin Packets in Wall Turbulence. In Self-Sustaining Mechanisms of Wall Turbulence (ed. R. L. Panton) (1998), 109-134 Computational Mechanics Publications, Southampton, UK.

Zhou, J., Adrian, R. J. and Balachandar, S., Autogeneration of Near-Wall Vortical Structures in Channel Flow. Physics of Fluids, 8 (1996), 288-290.

Zhou, J., Adrian, R. J., Balachandar, S. and Kendall, T. M., Mechanisms for Generating Coherent Packets of Hairpin Vortices in Near-Wall Turbulence, Journal of Fluid Mechanics, 387 (1999), 353-396.

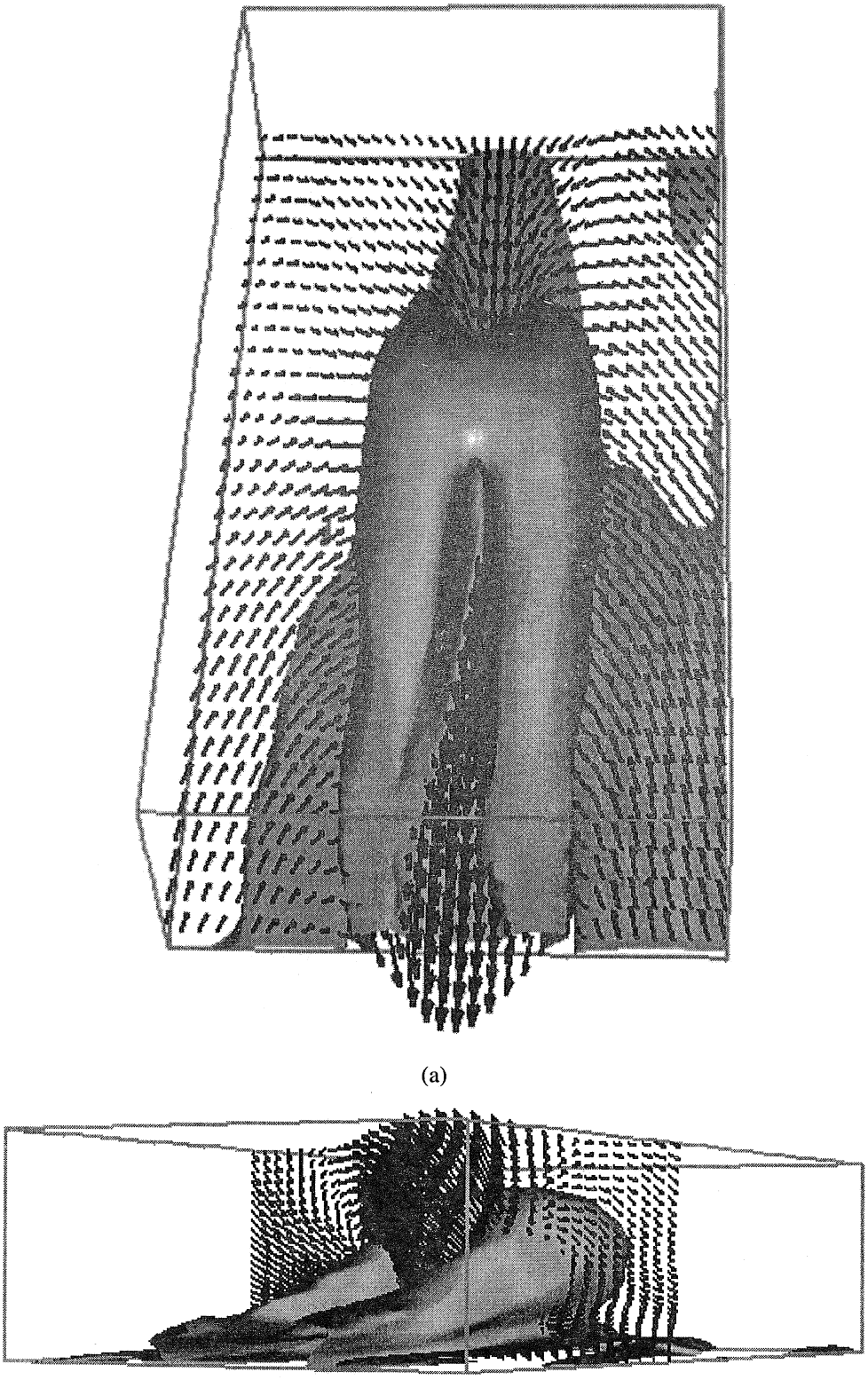

(a)

(b)

Fig. 1. Initial vortex found by conditionally averaging the velocity field around a Q2 event located at y+=50 in a Re_τ=300 channel flow. The surfaces are contours of the swirling strength.

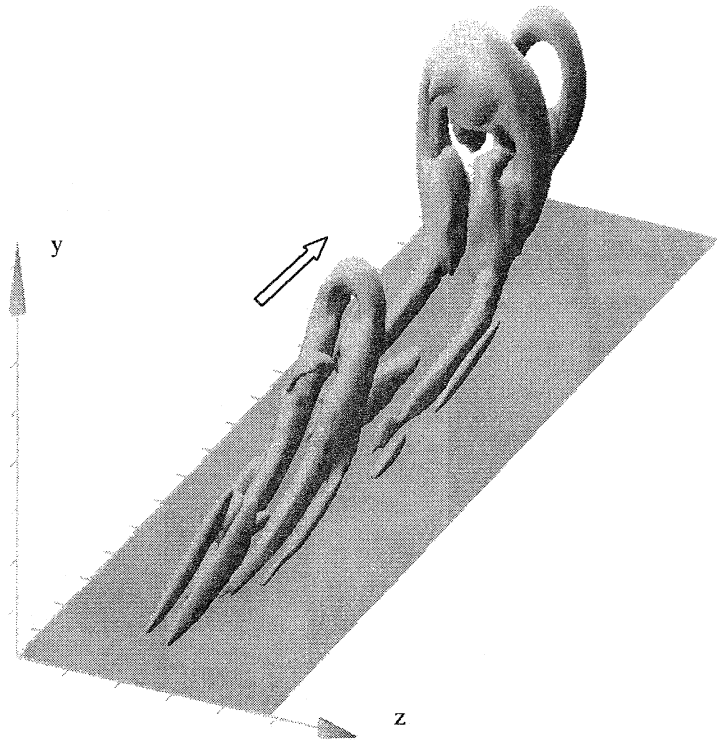

Fig. 2. The hairpin vortex packet that evolves from a symmetric primary hairpin as computed by DNS in Re_τ=150 channel flow. (*From Zhou, et al. 1999).* The surfaces are contours of the swirling strength.

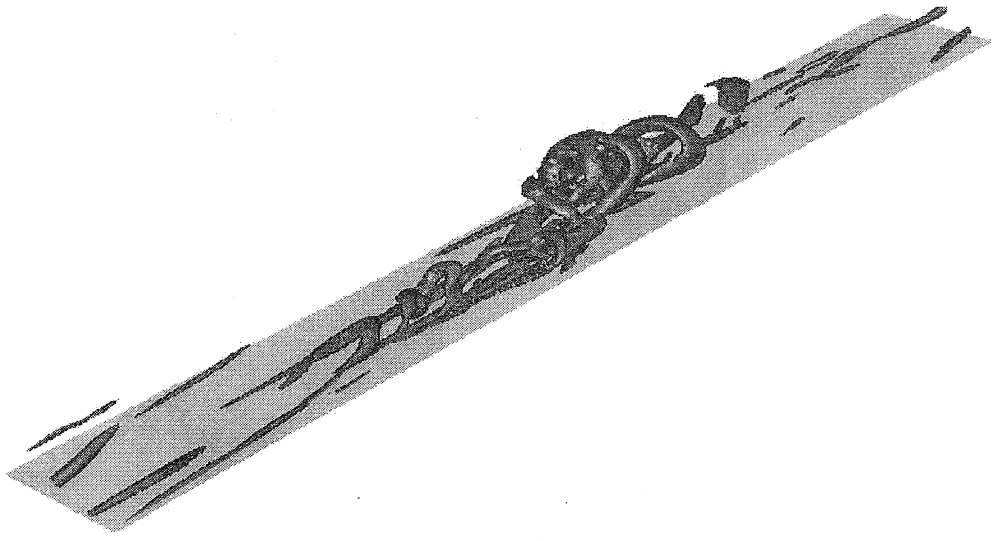

Fig. 3. The hairpin vortex packet that evolves in Re_τ=300 channel flow from the slightly asymmetric primary hairpin in Fig. 1. t^+=250. Note the complexity of this packet relative to the packet in Fig. 1. An animation of the evolution from the initial disturbance can be seen at **http://ltcf.tam.uiuc.edu**. The surfaces are contours of the swirling strength.

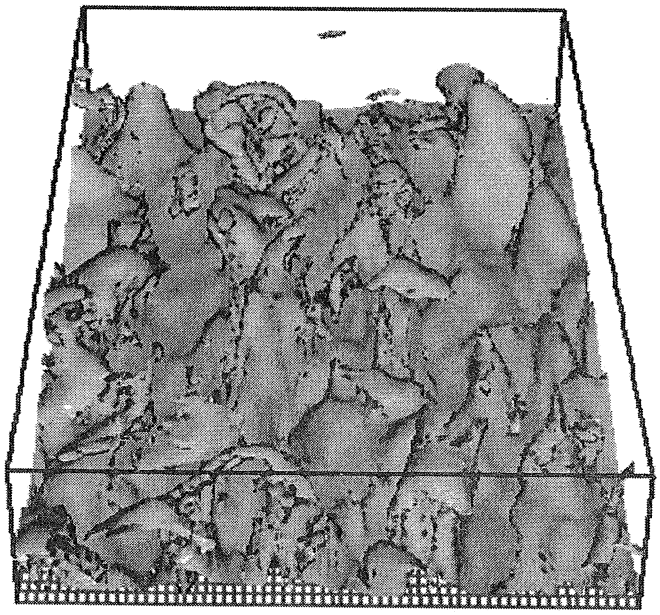

(a)

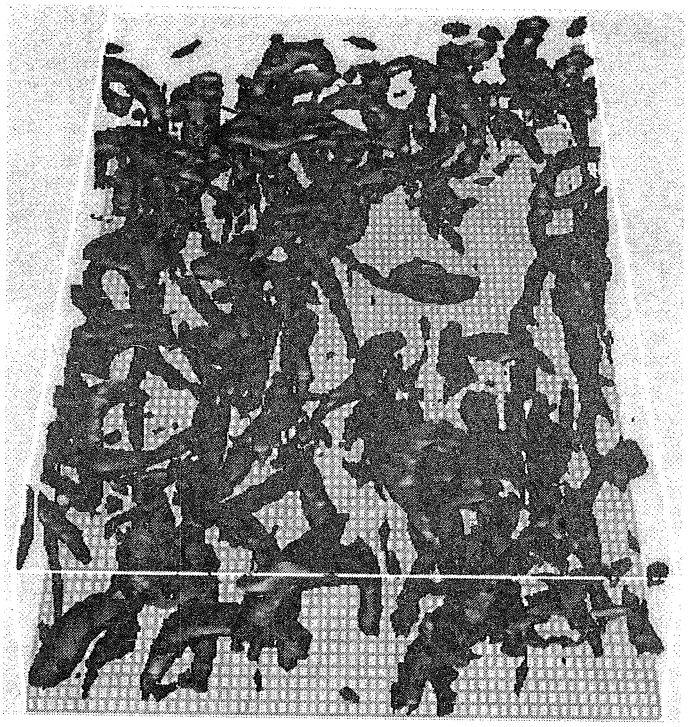

(b)

Fig. 4. A typical turbulent realization visualized on a sub-domain having dimensions $(L^+_x, L^+_y, L^+_z) = (950, 300, 475)$. (a) iso-surfaces of the enstrophy, $|\omega|$; (b) iso-surfaces of the swirling strength, λ_{ci}.

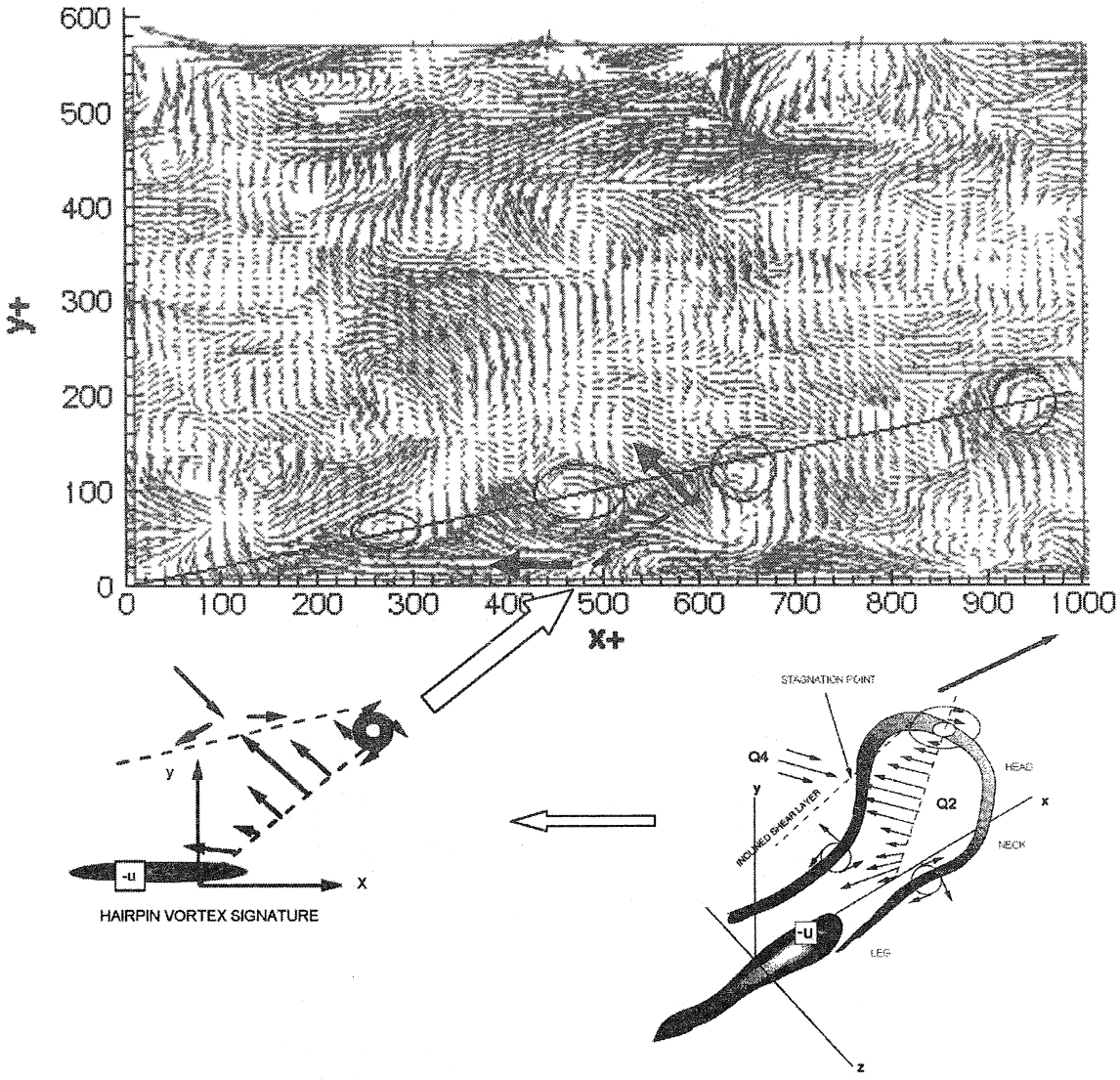

Fig. 5. A typical *x-y* cross-section of the channel flow. Note the presence of several patterns that match the hairpin vortex signature consisting of a vortex head atop an incline region of Q2 vectors lying downstream of a region of Q4 vectors that stagnate against the Q2 flow. One of the patterns is highlighted.

(a)

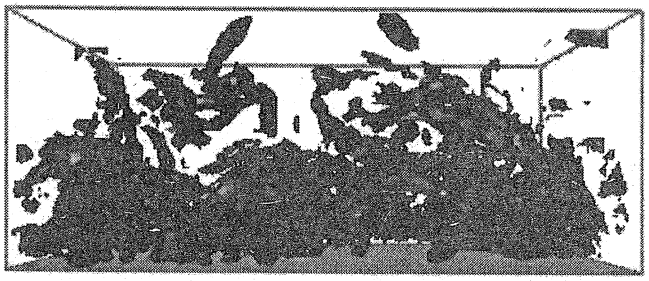

(b)

Fig. 6. (a) Side view of the channel flow in Fig. 4. (b) End view. The visualization is done using contours of the swirling strength, as in Fig. 4(b).

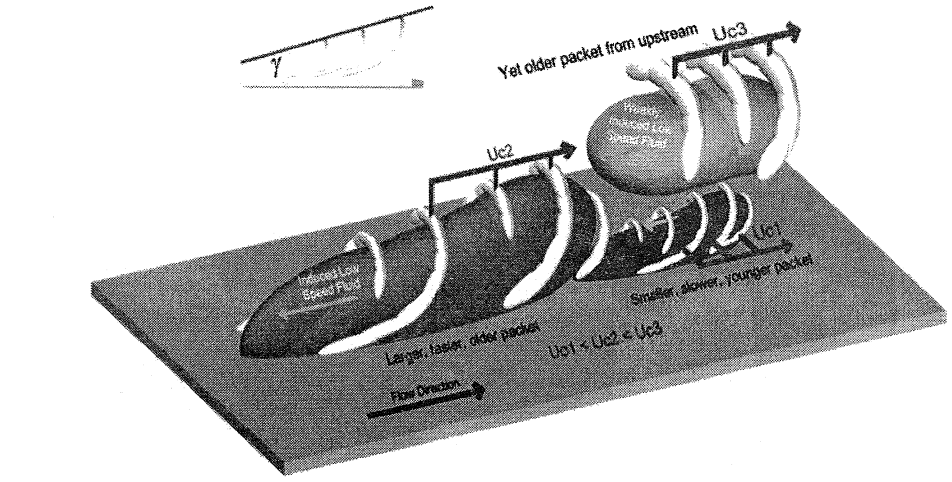

(a)

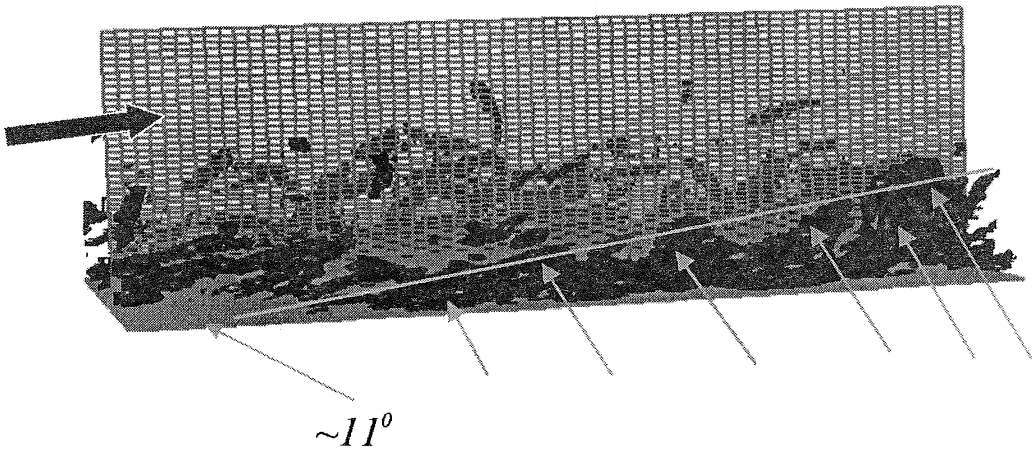

(b)

Fig. 7. (a) Schematic of the hairpin vortex packet model (*from Adrian, et al. 2000)*; (b) Hairpins identified by inspecting the side view of the velocity field in Fig. 6 using the template provided by the hairpin vortex signature.

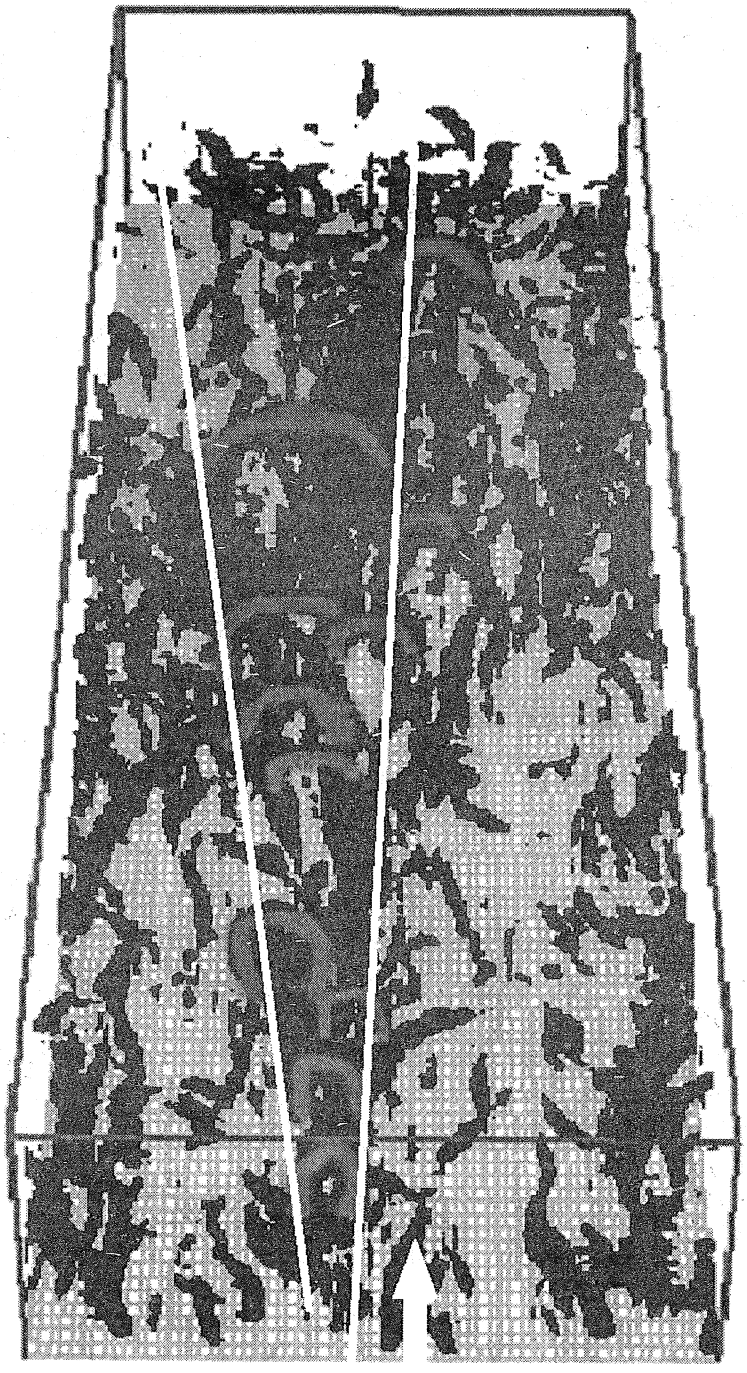

Fig. 7 (cont'd). (c) Oblique view of the hairpin packet formed from the vortices found in 6(b).

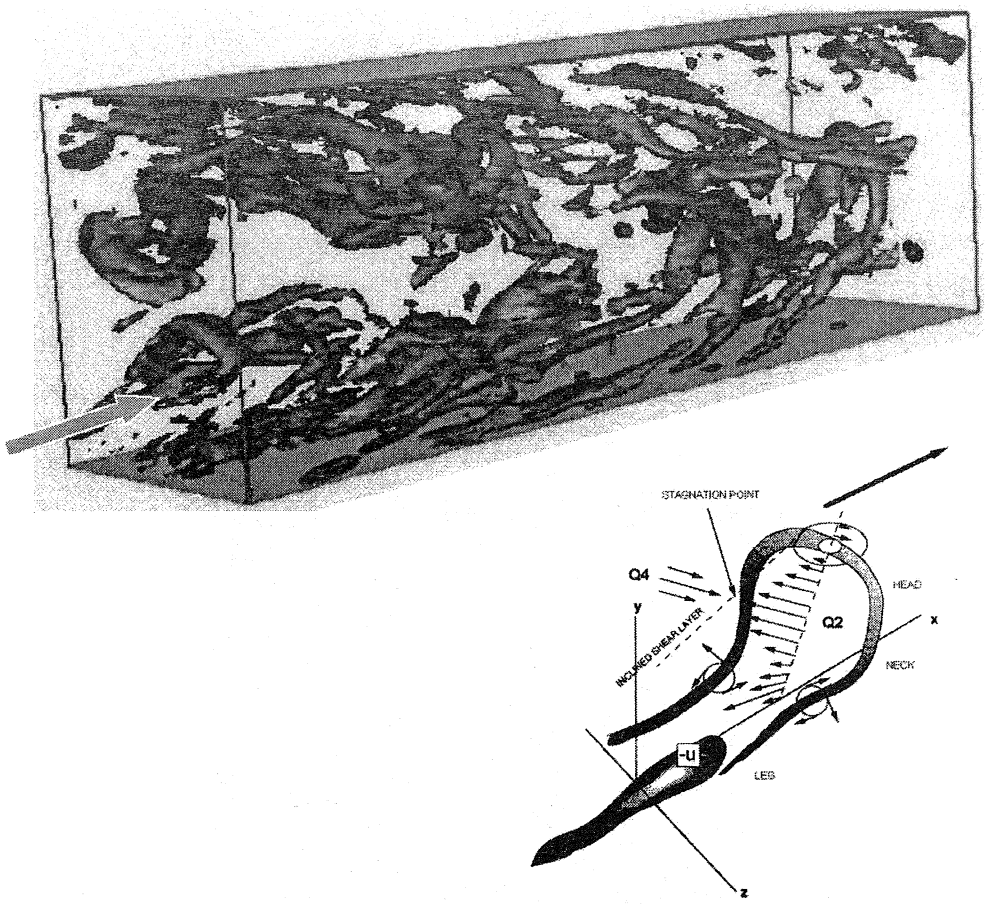

Fig. 8. Contours of swirling strength show hairpin packets growing from both the top and bottom walls of the channel.

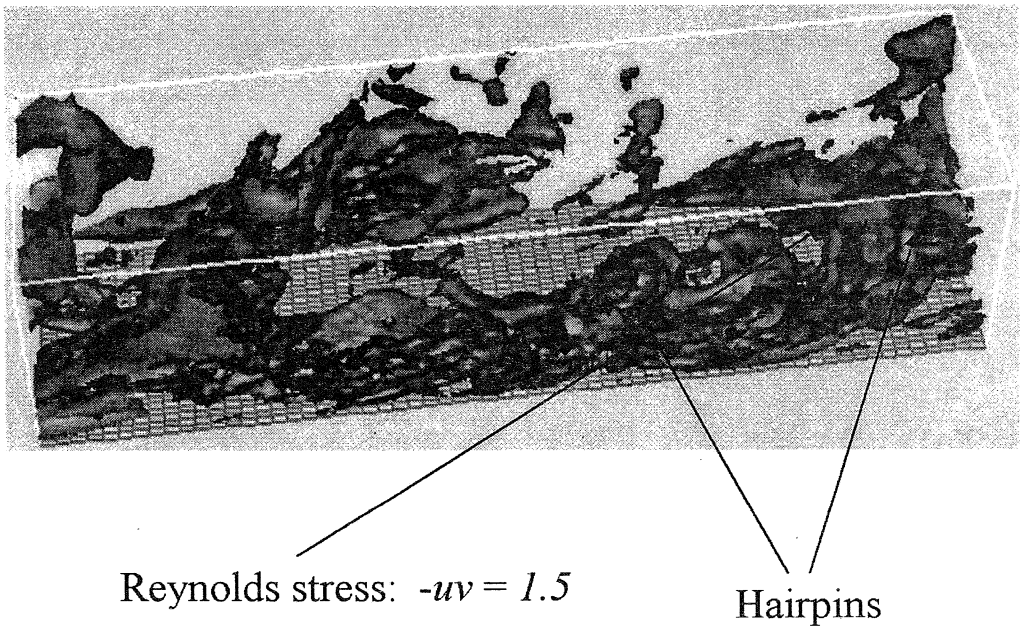

Fig. 9. The alignment of hairpins in the packets creates long streaks of Reynolds shear stress, accounting for much of the total turbulent friction.

List of Recent TAM Reports

No.	Authors	Title	Date
898	Students in TAM 293–294	Thirty-fourth student symposium on engineering mechanics (May 1997), J. W. Phillips, coordinator: Selected senior projects by M. R. Bracki, A. K. Davis, J. A. (Myers) Hommema, and P. D. Pattillo	Dec. 1998
899	Taha, A., and P. Sofronis	A micromechanics approach to the study of hydrogen transport and embrittlement—*Engineering Fracture Mechanics* **68**, 803–837 (2001)	Jan. 1999
900	Ferney, B. D., and K. J. Hsia	The influence of multiple slip systems on the brittle–ductile transition in silicon—*Materials Science Engineering A* **272**, 422–430 (1999)	Feb. 1999
901	Fried, E., and A. Q. Shen	Supplemental relations at a phase interface across which the velocity and temperature jump—*Continuum Mechanics and Thermodynamics* **11**, 277–296 (1999)	Mar. 1999
902	Paris, A. J., and G. A. Costello	Cord composite cylindrical shells: Multiple layers of cords at various angles to the shell axis	Apr. 1999
903	Ferney, B. D., M. R. DeVary, K. J. Hsia, and A. Needleman	Oscillatory crack growth in glass—*Scripta Materialia* **41**, 275–281 (1999)	Apr. 1999
904	Fried, E., and S. Sellers	Microforces and the theory of solute transport—*Zeitschrift für angewandte Mathematik und Physik* **51**, 732–751 (2000)	Apr. 1999
905	Balachandar, S., J. D. Buckmaster, and M. Short	The generation of axial vorticity in solid-propellant rocket-motor flows—*Journal of Fluid Mechanics* (submitted)	May 1999
906	Aref, H., and D. L. Vainchtein	The equation of state of a foam—*Physics of Fluids* **12**, 23–28 (2000)	May 1999
907	Subramanian, S. J., and P. Sofronis	Modeling of the interaction between densification mechanisms in powder compaction—*International Journal of Solids and Structures*, in press (2000)	May 1999
908	Aref, H., and M. A. Stremler	Four-vortex motion with zero total circulation and impulse—*Physics of Fluids* **11**, 3704-3715	May 1999
909	Adrian, R. J., K. T. Christensen, and Z.-C. Liu	On the analysis and interpretation of turbulent velocity fields—*Experiments in Fluids* **29**, 275–290 (2000)	May 1999
910	Fried, E., and S. Sellers	Theory for atomic diffusion on fixed and deformable crystal lattices—*Journal of Elasticity* **59**, 67–81 (2000)	June 1999
911	Sofronis, P., and N. Aravas	Hydrogen induced shear localization of the plastic flow in metals and alloys—*European Journal of Mechanics/A Solids* (submitted)	June 1999
912	Anderson, D. R., D. E. Carlson, and E. Fried	A continuum-mechanical theory for nematic elastomers—*Journal of Elasticity* **56**, 33–58 (1999)	June 1999
913	Riahi, D. N.	High Rayleigh number convection in a rotating melt during alloy solidification—*Recent Developments in Crystal Growth Research* **2**, 211–222 (2000)	July 1999
914	Riahi, D. N.	Buoyancy driven flow in a rotating low Prandtl number melt during alloy solidification—*Current Topics in Crystal Growth Research* **5**, 151–161 (2000)	July 1999
915	Adrian, R. J.	On the physical space equation for large-eddy simulation of inhomogeneous turbulence—*Physics of Fluids* (submitted)	July 1999
916	Riahi, D. N.	Wave and vortex generation and interaction in turbulent channel flow between wavy boundaries—*Journal of Mathematical Fluid Mechanics* (submitted)	July 1999
917	Boyland, P. L., M. A. Stremler, and H. Aref	Topological fluid mechanics of point vortex motions	July 1999
918	Riahi, D. N.	Effects of a vertical magnetic field on chimney convection in a mushy layer—*Journal of Crystal Growth* **216**, 501–511 (2000)	Aug. 1999

List of Recent TAM Reports (cont'd)

No.	Authors	Title	Date
919	Riahi, D. N.	Boundary mode–vortex interaction in turbulent channel flow over a non-wavy rough wall—*Proceedings of the Royal Society of London A*, in press (2001)	Sept. 1999
920	Block, G. I., J. G. Harris, and T. Hayat	Measurement models for ultrasonic nondestructive evaluation—*IEEE Transactions on Ultrasonics, Ferroelectrics, and Frequency Control* **47**, 604–611 (2000)	Sept. 1999
921	Zhang, S., and K. J. Hsia	Modeling the fracture of a sandwich structure due to cavitation in a ductile adhesive layer—*Journal of Applied Mechanics* (submitted)	Sept. 1999
922	Nimmagadda, P. B. R., and P. Sofronis	Leading order asymptotics at sharp fiber corners in creeping-matrix composite materials	Oct. 1999
923	Yoo, S., and D. N. Riahi	Effects of a moving wavy boundary on channel flow instabilities—*Theoretical and Computational Fluid Dynamics* (submitted)	Nov. 1999
924	Adrian, R. J., C. D. Meinhart, and C. D. Tomkins	Vortex organization in the outer region of the turbulent boundary layer—*Journal of Fluid Mechanics* **422**, 1–53 (2000)	Nov. 1999
925	Riahi, D. N., and A. T. Hsui	Finite amplitude thermal convection with variable gravity—*International Journal of Mathematics and Mathematical Sciences* **25**, 153–165 (2001)	Dec. 1999
926	Kwok, W. Y., R. D. Moser, and J. Jiménez	A critical evaluation of the resolution properties of *B*-spline and compact finite difference methods—*Journal of Computational Physics* (submitted)	Feb. 2000
927	Ferry, J. P., and S. Balachandar	A fast Eulerian method for two-phase flow—*International Journal of Multiphase Flow*, in press (2000)	Feb. 2000
928	Thoroddsen, S. T., and K. Takehara	The coalescence–cascade of a drop—*Physics of Fluids* **12**, 1257–1265 (2000)	Feb. 2000
929	Liu, Z.-C., R. J. Adrian, and T. J. Hanratty	Large-scale modes of turbulent channel flow: Transport and structure—*Journal of Fluid Mechanics* (submitted)	Feb. 2000
930	Borodai, S. G., and R. D. Moser	The numerical decomposition of turbulent fluctuations in a compressible boundary layer—*Theoretical and Computational Fluid Dynamics* (submitted)	Mar. 2000
931	Balachandar, S., and F. M. Najjar	Optimal two-dimensional models for wake flows—*Physics of Fluids*, in press (2000)	Mar. 2000
932	Yoon, H. S., K. V. Sharp, D. F. Hill, R. J. Adrian, S. Balachandar, M. Y. Ha, and K. Kar	Integrated experimental and computational approach to simulation of flow in a stirred tank—*Chemical Engineering Sciences* (submitted)	Mar. 2000
933	Sakakibara, J., Hishida, K., and W. R. C. Phillips	On the vortical structure in a plane impinging jet—*Journal of Fluid Mechanics* **434**, 273–300 (2001)	Apr. 2000
934	Phillips, W. R. C.	Eulerian space–time correlations in turbulent shear flows	Apr. 2000
935	Hsui, A. T., and D. N. Riahi	Onset of thermal–chemical convection with crystallization within a binary fluid and its geological implications—*Geochemistry, Geophysics, Geosystems* **2**, 2000GC000075 (2001)	Apr. 2000
936	Cermelli, P., E. Fried, and S. Sellers	Configurational stress, yield, and flow in rate-independent plasticity—*Proceedings of the Royal Society of London A* **457**, 1447–1467 (2001)	Apr. 2000
937	Adrian, R. J., C. Meneveau, R. D. Moser, and J. J. Riley	Final report on 'Turbulence Measurements for Large-Eddy Simulation' workshop	Apr. 2000
938	Bagchi, P., and S. Balachandar	Linearly varying ambient flow past a sphere at finite Reynolds number—Part 1: Wake structure and forces in steady straining flow	Apr. 2000
939	Gioia, G., A. DeSimone, M. Ortiz, and A. M. Cuitiño	Folding energetics in thin-film diaphragms	Apr. 2000

List of Recent TAM Reports (cont'd)

No.	Authors	Title	Date
940	Chaïeb, S., and G. H. McKinley	Mixing immiscible fluids: Drainage induced cusp formation	May 2000
941	Thoroddsen, S. T., and A. Q. Shen	Granular jets—*Physics of Fluids* **13**, 4–6 (2001)	May 2000
942	Riahi, D. N.	Non-axisymmetric chimney convection in a mushy layer under a high-gravity environment—In *Centrifugal Materials Processing* (L. L. Regel and W. R. Wilcox, eds.), 295–302 (2001)	May 2000
943	Christensen, K. T., S. M. Soloff, and R. J. Adrian	PIV Sleuth: Integrated particle image velocimetry interrogation/validation software	May 2000
944	Wang, J., N. R. Sottos, and R. L. Weaver	Laser induced thin film spallation—*Experimental Mechanics* (submitted)	May 2000
945	Riahi, D. N.	Magnetohydrodynamic effects in high gravity convection during alloy solidification—In *Centrifugal Materials Processing* (L. L. Regel and W. R. Wilcox, eds.), 317–324 (2001)	June 2000
946	Gioia, G., Y. Wang, and A. M. Cuitiño	The energetics of heterogeneous deformation in open-cell solid foams	June 2000
947	Kessler, M. R., and S. R. White	Self-activated healing of delamination damage in woven composites—*Composites A: Applied Science and Manufacturing* **32**, 683–699 (2001)	June 2000
948	Phillips, W. R. C.	On the pseudomomentum and generalized Stokes drift in a spectrum of rotational waves—*Journal of Fluid Mechanics* **430**, 209–229 (2001)	July 2000
949	Hsui, A. T., and D. N. Riahi	Does the Earth's nonuniform gravitational field affect its mantle convection?—*Physics of the Earth and Planetary Interiors* (submitted)	July 2000
950	Phillips, J. W.	Abstract Book, 20th International Congress of Theoretical and Applied Mechanics (27 August – 2 September, 2000, Chicago)	July 2000
951	Vainchtein, D. L., and H. Aref	Morphological transition in compressible foam—*Physics of Fluids* **13**, 2152–2160 (2001)	July 2000
952	Chaïeb, S., E. Sato-Matsuo, and T. Tanaka	Shrinking-induced instabilities in gels	July 2000
953	Riahi, D. N., and A. T. Hsui	A theoretical investigation of high Rayleigh number convection in a nonuniform gravitational field—*Acta Mechanica* (submitted)	Aug. 2000
954	Riahi, D. N.	Effects of centrifugal and Coriolis forces on a hydromagnetic chimney convection in a mushy layer—*Journal of Crystal Growth* **226**, 393–405 (2001)	Aug. 2000
955	Fried, E.	An elementary molecular-statistical basis for the Mooney and Rivlin–Saunders theories of rubber-elasticity—*Journal of the Mechanics and Physics of Solids*, in press (2001)	Sept. 2000
956	Phillips, W. R. C.	On an instability to Langmuir circulations and the role of Prandtl and Richardson numbers—*Journal of Fluid Mechanics*, in press (2001)	Sept. 2000
957	Chaïeb, S., and J. Sutin	Growth of myelin figures made of water soluble surfactant—Proceedings of the 1st Annual International IEEE–EMBS Conference on Microtechnologies in Medicine and Biology (October 2000, Lyon, France), 345–348	Oct. 2000
958	Christensen, K. T., and R. J. Adrian	Statistical evidence of hairpin vortex packets in wall turbulence—*Journal of Fluid Mechanics* **431**, 433–443 (2001)	Oct. 2000
959	Kuznetsov, I. R., and D. S. Stewart	Modeling the thermal expansion boundary layer during the combustion of energetic materials—*Combustion and Flame*, in press (2001)	Oct. 2000
960	Zhang, S., K. J. Hsia, and A. J. Pearlstein	Potential flow model of cavitation-induced interfacial fracture in a confined ductile layer—*Journal of the Mechanics and Physics of Solids* (submitted)	Nov. 2000

List of Recent TAM Reports (cont'd)

No.	Authors	Title	Date
961	Sharp, K. V., R. J. Adrian, J. G. Santiago, and J. I. Molho	Liquid flows in microchannels—Chapter 6 of *CRC Handbook of MEMS* (M. Gad-el-Hak, ed.) (2001)	Nov. 2000
962	Harris, J. G.	Rayleigh wave propagation in curved waveguides—*Wave Motion*, in press (2001)	Jan. 2001
963	Dong, F., A. T. Hsui, and D. N. Riahi	A stability analysis and some numerical computations for thermal convection with a variable buoyancy factor—*Geophysical and Astrophysical Fluid Dynamics* (submitted)	Jan. 2001
964	Phillips, W. R. C.	Langmuir circulations beneath growing or decaying surface waves—*Journal of Fluid Mechanics* (submitted)	Jan. 2001
965	Bdzil, J. B., D. S. Stewart, and T. L. Jackson	Program burn algorithms based on detonation shock dynamics—*Journal of Computational Physics* (submitted)	Jan. 2001
966	Bagchi, P., and S. Balachandar	Linearly varying ambient flow past a sphere at finite Reynolds number: Part 2—Equation of motion—*Journal of Fluid Mechanics* (submitted)	Feb. 2001
967	Cermelli, P., and E. Fried	The evolution equation for a disclination in a nematic fluid—*Proceedings of the Royal Society A*, in press (2001)	Apr. 2001
968	Riahi, D. N.	Effects of rotation on convection in a porous layer during alloy solidification—Chapter in *Transport Phenomena in Porous Media* (D. B. Ingham and I. Pop, eds.), Oxford: Elsevier Science (2001)	Apr. 2001
969	Damljanovic, V., and R. L. Weaver	Elastic waves in cylindrical waveguides of arbitrary cross section—*Journal of Sound and Vibration* (submitted)	May 2001
970	Gioia, G., and A. M. Cuitiño	Two-phase densification of cohesive granular aggregates	May 2001
971	Subramanian, S. J., and P. Sofronis	Calculation of a constitutive potential for isostatic powder compaction—*International Journal of Mechanical Sciences* (submitted)	June 2001
972	Sofronis, P., and I. M. Robertson	Atomistic scale experimental observations and micromechanical/continuum models for the effect of hydrogen on the mechanical behavior of metals—*Philosophical Magazine* (submitted)	June 2001
973	Pushkin, D. O., and H. Aref	Self-similarity theory of stationary coagulation—*Physics of Fluids* (submitted)	July 2001
974	Lian, L., and N. R. Sottos	Stress effects in ferroelectric thin films—*Journal of the Mechanics and Physics of Solids* (submitted)	Aug. 2001
975	Fried, E., and R. E. Todres	Prediction of disclinations in nematic elastomers—*Proceedings of the National Academy of Sciences* (submitted)	Aug. 2001
976	Fried, E., and V. A. Korchagin	Striping of nematic elastomers—*International Journal of Solids and Structures* (submitted)	Aug. 2001
977	Riahi, D. N.	On nonlinear convection in mushy layers: Part I. Oscillatory modes of convection—*Journal of Fluid Mechanics* (submitted)	Sept. 2001
978	Sofronis, P., I. M. Robertson, Y. Liang, D. F. Teter, and N. Aravas	Recent advances in the study of hydrogen embrittlement at the University of Illinois—Invited paper, Hydrogen–Corrosion Deformation Interactions (Sept. 16–21, 2001, Jackson Lake Lodge, Wyo.)	Sept. 2001
979	Fried, E., M. E. Gurtin, and K. Hutter	A void-based description of compaction and segregation in flowing granular materials—*Proceedings of the Royal Society of London A* (submitted)	Sept. 2001
980	Adrian, R. J., S. Balachandar, and Z.-C. Liu	Spanwise growth of vortex structure in wall turbulence—Korean Society of Mechanical Engineers special issue on Flow Visualization (December 2001)	Sept. 2001
981	Adrian, R. J.	Information and the study of turbulence and complex flow—*Japanese Society of Mechanical Engineers B* (submitted)	Oct. 2001
982	Adrian, R. J., and Z.-C. Liu	Observation of vortex packets in direct numerical simulation of fully turbulent channel flow—*Journal of Visualization* (submitted)	Oct. 2001